Hypoimmunogenic Human Pluripotent Stem Cells are Valid Cell Sources for Cell Therapeutics with Normal Self-Renewal and Multi-Lineage Differentiation Capacity

Yifan Chen
Tongji University School of Medicine
Yanjie Zhou
Tongji University School of Medicine
Zhongshu Zhou
Tongji University School of Medicine
Jie Xiong
Tongji University School of Medicine
Yujiang Fang
Tongji University School of Medicine
Lin Ma
Tongji University School of Medicine
Ling Liu
Tongji University School of Medicine
Xiaoqing Zhang (xqzhang@tongji.edu.cn)
Tongji University School of Medicine https://orcid.org/0000-0002-7405-1893

Research Article

Keywords: hypoimmunogenic hPSCs, self-renewal, multilineage differentiation, functional maturity

Posted Date: February 4th, 2022

DOI: https://doi.org/10.21203/rs.3.rs-1297785/v1

Version of Record: A version of this preprint was published at Stem Cell Research & Therapy on January 24th, 2023. See the published version at https://doi.org/10.1186/s13287-022-03233-z.

Abstract

Hypoimmunogenic human pluripotent stem cells (hPSCs) are expected to serve as an unlimited cell source for generating universally compatible “off-the-shelf” cell grafts. However, whether the engineered hypoimmunogenic hPSCs still preserve their advantages of unlimited self-renewal and multilineage differentiation to yield functional tissue cells remains unclear. Here, we systematically studied the self-renewal and differentiation potency into functional tissue cells of three types of hypoimmunogenic hPSCs, established through biallelic lesion of B2M gene to remove all surface expression of classical and nonclassical HLA class I molecules ($B2M^{null}$), biallelic homologous recombination of nonclassical HLA-G1 to the B2M loci to knockout B2M while express membrane-bound β2m-HLA-G1 fusion proteins ($B2M^{mHLAG}$), and ectopic expression of soluble and secreted β2m-HLA-G5 fusion proteins in $B2M^{mHLAG}$ hPSCs ($B2M^{m/sHLAG}$). Our results show that hypoimmunogenic hPSCs with variable expression patterns of HLA molecules and immune compromising spectrums retain their normal self-renewal capacity and three germ-layer differentiation potency. More importantly, as exemplified by neurons, cardiomyocytes and hepatocytes, hypoimmunogenic hPSC-derived tissue cells are fully functional as of their morphology, electrophysiological properties, macromolecule transportation and metabolic regulation. Taken together, our findings indicate that engineered hypoimmunogenic hPSCs hold great promise of serving as an unlimited universal cell source for cell therapeutics.

Introduction

Human pluripotent stem cells (hPSCs), including human embryonic stem cells (hESCs) and human induced pluripotent stem cells (hiPSCs), are valuable cell sources for regenerative strategies as they can generate an unlimited amount of progeny cells or functional cells of interest [1–3]. Although autologous iPSCs-derived midbrain dopaminergic progenitor transplantation for treatment of Parkinson’s disease has yielded amazing outcomes in Parkinsonian monkeys and even patient, this individualized strategy is laborious, costly, and is only practical for chronic diseases [4–6]. Thus, engineering universal hypoimmunogenic hESCs or hiPSCs for allogeneic cell therapies targeting large patient populations could be more economically feasible and avoid long-term immunosuppressive interventions [7–9].

Both innate immune responses and adaptive immune responses are involved in allograft rejection [10]. HLA-E, the non-classical human leukocyte antigen (HLA) molecule, is a ligand for the inhibitory CD94/NGK2A complex expressed on partial NK cells [11–12]. HLA-G, another inhibitory ligand expressed at the maternal-fetal interface during pregnancy, acts as a better candidate to fully overcome rejection responses mediated by NK cells or macrophages [13–14]. Hence, overexpression of membrane-bound HLA-E and HLA-G1 or secreted HLA-G5 has been reported to efficiently inhibit NK cell-mediated allograft rejection [15–17]. Ectopic expression of CD47 in hPSCs, a “don’t-eat-me” signal that prevents cells from being engulfed by macrophages, also leads to low immunogenicity [16, 18–19].

Although targeting NK cell- and macrophage-involved innate immune responses restrain the immunogenicity, most immune-compromise interventions have been designed in hPSCs by targeting T

cell-mediated adaptive immune responses. HLA class I molecules, such as HLA-A, -B and -C, which are expressed on almost all nucleated cells and platelets, present intracellularly processed peptides to $CD8^+$ cytotoxic T cells and enable elimination of antigen-expressing or virus-infected cells [20]. HLA class I molecule is composed of highly polymorphic heavy chain alpha and β2-microglobulin (B2M). The β2-microglobulin forms a heterodimer with HLA class I proteins and is required for HLA class I expression on the cell surface. Thus, knockout of the B2M gene can restrict an immune response from cytotoxic $CD8^+$ T cells by depleting all HLA class I molecules [16, 21–26]. Meanwhile, cytotoxic T lymphocyte antigen 4 (CTLA4) and programmed death ligand-1 (PD-L1) are critical immune inhibitory molecules in maintaining peripheral tolerance through restraining T cell activity. Consequently, overexpression of CTLA4-immunoglobulin and PD-L1 in hPSCs has been shown to prevent allogenic immune rejection via blocking T cell checkpoint [27].

We have previously reported that although knockout of B2M gene in hPSCs ($B2M^{null}$) remarkably ameliorates T cell activation and T cell-mediated cytotoxicity, the deletion of B2M propagates NK cell activation and overrepresentation in allografts. Knockin of HLA-G1 within the frame of endogenous B2M loci biallelically ($B2M^{mHLAG}$) to express membrane-bound β2m-HLA-G1 fusion proteins while concomitantly ablate free β2m expression in the hPSCs largely abolishes immune rejections caused by T cells, NK cells and macrophages. Overexpression of soluble and secreted form of β2m-HLA-G5 fusion protein in $B2M^{mHLAG}$ hPSCs ($B2M^{m/sHLAG}$) would construct super hypoimmunogenic hPSCs, ensuring a low immunogenic environment with reduced expression of inflammatory cytokines in the allografts [17]. Of note, HLA molecules are expressed in hPSCs and their expressions moderately increase alongside *in vivo* development and *in vitro* differentiation [28–30]. Besides, HLA analog molecules in mice (major histocompatibility complex, MHC) play a role in synaptic plasticity during development [31–36] and B2M knockout mice have increased intestinal iron absorption and iron overload in the liver [37]. This arises an important while unaddressed question about whether the engineered hypoimmunogenic hPSCs still preserve their advantages of unlimited self-renewal and multilineage differentiation to yield functional tissue cells. To address this concern, in this study, we systematically studied the self-renewal capacity and differentiation potency into functional tissue cells of $B2M^{null}$, $B2M^{mHLAG}$ and $B2M^{m/sHLAG}$, three types of hypoimmunogenic hPSCs. Our results show that hypoimmunogenic hPSCs with variable expression patterns of HLA molecules and immune compromising spectrums retain their normal self-renewal capacity and could be efficiently differentiated into functional and mature lineage cells, such as electrophysiologically active neurons, beating cardiomyocytes and albumin secreting hepatocytes.

Results

Hypoimmunogenic hPSCs could be long-term maintained in culture and keep three germinal differentiation potency

We constructed hypoimmunogenic hPSCs with different strategies, biallelic lesion of B2M gene to remove all surface expression of classical and nonclassical HLA class I molecules ($B2M^{null}$), biallelic

homologous recombination of nonclassical HLA-G1 to the B2M loci to knockout B2M while express membrane-bound β2m-HLA-G1 fusion proteins ($B2M^{mHLAG}$), and ectopic expression of soluble and secreted β2m-HLA-G5 fusion proteins in $B2M^{mHLAG}$ hPSCs ($B2M^{m/sHLAG}$). hPSCs constructed with these three strategies have shown robust immunotolerance to $CD8^+$ T cells and NK cells both *in vitro* and *in vivo* allografts [17].

To study whether these engineered hypoimmunogenic hPSCs retain normal self-renewal and differentiation potency, we continuously cultured these cells to more than 30 passages. After passage, all three hypoimmunogenic hPSCs exhibited typical morphology with large nuclear/cytoplasmic ratios, multiple and prominent nucleoli, and round colonies with clear edges resembling of the wild type (WT) control (Fig. 1A). Immunostaining experiments revealed that all three hypoimmunogenic hPSCs had uniform nuclear expression of typical pluripotent transcription factors, including OCT4 and SOX2 (Fig. 1B). These data suggest that hypoimmunogenic hPSCs engineered with different strategies retained their pluripotency and could be finely maintained in culture. To transcriptionally characterize the engineered hypoimmunogenic hPSCs, we performed RNA-seq analyses on these cells at passage 55. Dimensionality reduction and clustering by principal component analysis (PCA) demonstrated that hypoimmunogenic hPSCs were clustered with WT hPSCs, but not *in vivo* differentiated teratomas (Fig. 1C, 1D). Moreover, similar to the WT control, all three hypoimmunogenic hPSCs showed robust expression of pluripotency genes while lack of expression of three germ layer-featured genes (Fig. 1E), highlighting a non-differentiated state of these hypoimmunogenic hPSCs.

To investigate their differentiation potency, three types of hypoimmunogenic hPSCs were subcutaneously injected into non-obese diabetic/severe combined immune-deficient (NOD/SCID) mice, with the WT hPSCs as a control, respectively. For all four groups, teratomas were visibly formed at similar occurrence rates after 2 months of injection. Teratomas were then resected, fixed in paraformaldehyde, followed by hematoxylin-eosin (H&E) staining (Fig. 1C). We observed ectodermal neural tube-like tissues, mesoderm-derived cartilage like tissues and endodermal intestine like tissues in both WT- and the three types of hypoimmunogenic hPSCs-injected groups. The dissected teratomas from all groups were also subjected to RNA-seq. Heatmap analyses revealed that teratomas from all three hypoimmunogenic hPSCs and WT hPSCs had similar gene expression patterns featured with all three germ layers (Fig. 1E). Of note, similar to the WT control, we did not observe elevated pluripotent marker genes in any teratomas derived from the three hypoimmunogenic hPSCs. Together, these results suggest that the hypoimmunogenic hPSCs with various HLA expression patterns and immune compromising spectrums could be efficiently differentiated into all three germ layers.

Neurons differentiated from hypoimmunogenic hPSCs functionally mature and form neural circuits

To study whether hypoimmunogenic hPSCs could be efficiently specified into functional tissue cells, we firstly differentiated WT hPSCs and all three hypoimmunogenic hPSCs toward cortical neurons via the Dual-Smad inhibition differentiation protocol as previously described [38–40] (Fig. 2A). Neural ectoderm (NE) cells appeared on post-differentiation day 7 and they formed typical neural tube-like rosettes on day

10 in all four groups. Immunostaining experiments showed that on day 10, most NE cells were positive for PAX6 (Fig. 2B), indicating synchronized neural induction in control and hypoimmunogenic hPSC groups. Quantification of the percentage of $PAX6^+$ cells in NE cultures further strengthened the conclusion that hypoimmunogenic hPSCs were almost uniformly specified into the $PAX6^+$ NE (Fig. 2C).

The specified NE were further differentiated into neural precursors and then to neurons (Fig. 2A). On post-differentiation day 30, neurons yielded from all three hypoimmunogenic hPSCs were positive for TUJ1 with extended long projections (Fig. 2D). The differentiated neurons from hypoimmunogenic hPSCs also expressed punctated synapsin1 (SYN1), a hallmark protein of presynaptic membrane, at 8 weeks post differentiation (Fig. 2D), indicating gradual synaptic maturation of WT and hypoimmunogenic hPSC-derived neurons.

To characterize the functional maturity of the three hypoimmunogenic hPSC-derived neurons, whole-cell patch-clamp electrophysiological recording experiments were performed. All three hypoimmunogenic hPSC-derived neurons had the ability to fire action potentials (APs) repetitively in response to current injection (Fig. 2E, 2F). AP properties were then quantified and compared to evaluate the electrophysiological maturity of the neurons. The resting membrane potentials (RMPs) of WT-, $B2M^{null}$-, $B2M^{mHLAG}$- and $B2M^{m/sHLAG}$-derived neurons were -57.18±2.510 mV, -55.50±1.564 mV, -61.58±4.026 mV, and -58.27±3.627 mV, respectively. The peak amplitudes were 83.70±2.386 mV, 79.26±6.053 mV, 95.16±6.068 mV, and 95.50±7.588 mV, respectively. There were no significant differences in all four groups by analyzing these AP parameters (Fig. 2G, 2H), indicating that the hypoimmunogenic hPSC-derived neurons attained the capacity to fire trains-of-action potentials by 8-10 weeks, the same time point for neurons derived from the WT hPSCs. In addition, there were no differences in synaptic connectivity amongst the WT and hypoimmunogenic hPSC-derived neurons (Fig. 2I, 2J, 2K). The frequencies of spontaneous synaptic activity from WT-, $B2M^{null}$-, $B2M^{mHLAG}$- and $B2M^{m/sHLAG}$-derived neurons were 1.33±0.4024 Hz, 4.032±1.676 Hz, 0.8269±0.2159 Hz, and 0.6134±0.1601 Hz, respectively. The amplitudes of spontaneous synaptic activity were 28.46±8.173 pA, 29.63±4.473 pA, 50.98±7.815 pA, and 48.94±21.18 pA, respectively. Taken together, these data suggest that the three types of hypoimmunogenic hPSCs are normally programmed into electrophysiologically mature neurons in culture.

Hypoimmunogenic hPSC-derived cardiomyocytes spontaneously contract and possess functionally electrophysiological characteristics

Cardiomyocyte transplantation has been considered as a replacement for heart transplantation and conventional regenerative therapies [41–43]. To study whether hypoimmunogenic hPSCs hold the ability to differentiate into functional and mature cardiomyocytes, WT, $B2M^{null}$, $B2M^{mHLAG}$ and $B2M^{m/sHLAG}$ hPSCs were differentiated toward a cardiomyocyte fate with a well-characterized protocol [44–45] (Fig. 3A). On day 8, cells differentiated from WT and all three hypoimmunogenic hPSCs were uniformly positive for NKX2.5, a cardiac transcription factor, suggesting synchronized cardiac fate specification (Fig. 3B). On day 12, cardiomyocytes derived from hypoimmunogenic hPSCs as well as WT hPSCs began

to spontaneously contract, and these cardiomyocytes beat robustly even after 100 days of differentiation (**Supplementary video 1-4**). The hypoimmunogenic hPSC-derived cardiomyocytes were also positive for cardiac troponin T (cTnT), a highly cardiac-specific myofilament protein. Quantification studies revealed that the percentage of $cTnT^+$ cardiomyocytes in the entire culture of WT and all three hypoimmunogenic hPSCs were over 95% with batch-to-batch consistency (Fig. 3B, 3C). To evaluate the cardiac sarcomere organization, cells were labeled with α-actinin, the Z-line marker of the sarcomere, and myosin light chain 2 atrial isoform (MLC2a), the A-band marker of the sarcomere, separately. Again, hypoimmunogenic hPSC-derived cardiomyocytes showed typical α-actinin and MLC2a staining (Fig. 3D). Taken together, immunolabeling of multiple myofilament proteins indicates that a well-organized sarcomeric structure can be similarly developed in all three hypoimmunogenic hPSC-derived cardiomyocytes.

To assess the maturity of cardiomyocytes derived from hypoimmunogenic hPSCs, we performed electrophysiological studies in cardiomyocytes derived from WT, $B2M^{null}$, $B2M^{mHLAG}$ and $B2M^{m/sHLAG}$ hPSCs 30-35 days post differentiation, a time window when ventricular-like cells being the predominant phenotype [46]. A majority of hypoimmunogenic hPSC-derived cardiomyocytes exhibited spontaneous ventricular-like electrical activity, similarly to Burridge's report [46]. Representative recordings of ventricular-like action potentials were shown in Fig. 3E. Specifically, the RMPs of WT-, $B2M^{null}$-, $B2M^{mHLAG}$- and $B2M^{m/sHLAG}$-derived ventricular-like cells were -55.30±1.398 mV, -55.60±2.230 mV, -56.64±1.421 mV, and -56.65±1.779 mV, respectively. The action potential amplitudes (APAs) of WT-, $B2M^{null}$-, $B2M^{mHLAG}$- and $B2M^{m/sHLAG}$-derived ventricular-like cells were 101.0±1.610 mV, 97.39±1.530 mV, 95.52±2.343 mV, and 100.9±1.935 mV, respectively. The action potential durations (APDs) at different levels of repolarization (90% and 50%, APD90 and APD50) of WT-, $B2M^{null}$-, $B2M^{mHLAG}$- and $B2M^{m/sHLAG}$-derived ventricular-like cells were 221.6±35.50 ms and 173.7±25.68 ms, 288.1±27.89 ms and 233.2±25.85 ms, 278.9±21.61 ms and 213.3±16.27 ms, and 191.7±13.72 and 144.0±11.20 ms, respectively. The maximal rates of depolarization (dV/dtmax) of WT-, $B2M^{null}$-, $B2M^{mHLAG}$- and $B2M^{m/sHLAG}$-derived ventricular-like cells were 17.70±2.163 V/s, 20.70±4.778 V/s, 17.46±3.062 V/s, and 15.46±1.509 V/s, respectively. Quantification data of the AP properties of ventricular cells derived from each group were presented and they showed no significant differences among groups (Fig. 3F, 3G, 3H, 3I, 3J). These data suggest that the engineered hypoimmunogenic hPSCs by modifying HLA class I molecules could be faithfully differentiated into functionally mature cardiomyocytes with proper cytoskeleton morphology and electrophysiological activities.

Hypoimmunogenic Hpscs Differentiate Into Hepatocytes With Featured Metabolic Functions

Various from neurons and cardiomyocytes, which are typical for their induced or spontaneous electrophysiological excitability, hepatocytes have more complex cellular functions related to metabolic pathways, such as cargo transport, insulin-regulated glucose metabolism, and detoxification. We used a four-step protocol to drive hPSCs toward a definitive endoderm and then a hepatocyte fate [47–48] (Fig. 4A). Immunostaining experiments revealed that the vast majority of the differentiation derivatives from WT and all three hypoimmunogenic hPSCs were positive for alpha fetoprotein (AFP) on day 13 (Fig. 4B), suggesting a uniform hepatic precursor fate (HPCs) obtained in all cultures. On day 21, albumin

(ALB), a marker of mature hepatocytes, was detected in hepatocyte-like cells (Fig. 4B). FACS analysis revealed that ~90% cells were positive for ALB in WT and all three hypoimmunogenic hPSCs cultures (Fig. 4C). These results suggest that hypoimmunogenic hPSCs are successfully specified into hepatocytes with high efficiency resembling those of the WT hPSCs.

ALB synthesis assays were further performed to specifically test the metabolic activities of differentiated hepatocytes. The concentrations of secreted ALB in the supernatants of day 21 hepatocytes cultures from WT, $B2M^{null}$, $B2M^{mHLAG}$ and $B2M^{m/sHLAG}$ hPSCs were 20.40±0.631 μg/ml, 22.18±2.424 μg/ml, 19.31±0.927 μg/ml, and 20.95±1.763 μg/ml, respectively, with no obvious differences within each group (Fig. 4D). Indocyanine green (ICG) uptake and release assays showed that all three hypoimmunogenic hPSC-derived hepatocytes exhibited clear ICG uptake and release within 6 h similar to the WT control (Fig. 4E). In addition, periodic acid schiff (PAS) staining revealed comparable glycogen storage in all four groups (Fig. 4F). These results indicate that functional hepatocyte-like cells can be derived from hypoimmunogenic hPSCs, and these hypoimmunogenic hPSCs-derived cells have regular metabolic functions, such as macromolecule transportation and glucose metabolism.

Discussion

In this study, we explored the self-renewal capacity and the functionality of their differentiated tissue cells of hypoimmunogenic hPSCs with different HLA class I presentation patterns. The $B2M^{null}$ hPSCs lack surface expression of classical and nonclassical HLA class I molecules. The $B2M^{mHLAG}$ hPSCs and the $B2M^{m/sHLAG}$ hPSCs are designed to simulate HLA class I presentation pattern in maternal-fetal interface, which lack cell surface expression of classical HLA class I molecules, but have membrane-bound β2m-HLA-G1 fusion proteins expression and the latter of which have ectopic expression of soluble and secreted β2m-HLA-G5. We present here promising evidences to show that all three hypoimmunogenic hPSCs retain their normal self-renewal capacity and could be efficiently differentiated into functional and mature lineage cells, including electrophysiologically active neurons, beating cardiomyocytes and albumin secreting hepatocytes. To our knowledge, this is the first research to systematically study and address the question of whether the engineered hypoimmunogenic hPSCs with variable expression patterns of HLA molecules and immune compromising spectrums still preserve their advantages of unlimited self-renewal and multilineage differentiation to yield functional tissue cells, which paves the way for future applications of these engineered cells for cell therapeutics.

Here, we reveal that the $B2M^{null}$, $B2M^{mHLAG}$ and $B2M^{m/sHLAG}$ hPSCs have typical morphology and can be long-term maintained in culture with no differences observed from that of the WT hPSCs. RNA-seq analyses show that hypoimmunogenic hPSCs and WT hPSCs have similar gene expression profiles. Meanwhile, these hypoimmunogenic hPSCs could be targeted to ectodermal, mesodermal and endodermal lineages, as exemplified by neural precursors, cardiac precursors and hepatic precursors, with high efficiency. Teratomas yielded from hypoimmunogenic hPSCs and WT hPSCs harbor lineages of all three germ layers and transcriptional profiling studies elucidate that they are comparable of upregulation

of featured genes related to all three germ layers and downregulation of genes related to pluripotency. These evidences firmly secure the conclusion that all three hypoimmunogenic hPSCs are phenotypically normal in pluripotency maintenance and three germ-layer differentiation. It is reported that classical HLA class I molecules are expressed in hPSCs and their expression moderately increase alongside *in vivo* development and *in vitro* differentiation [28–30]. Given knockout of B2M does not interfere with hPSCs self-renewal or three germ-layer differentiation, this indicates that expression of HLA class I molecules on the surface of hPSCs is not intrinsically required for their function. HLA-G is not present in hPSCs [28]. Here, we show that ectopic expression of either membrane-bound or secreted HLA-G in hPSCs has no effect on their normal self-renewal and three germ-layer differentiation capacity, coinciding with their early physiological expression at the fetomaternal interface in cytotrophoblasts during embryonic development [13–14].

Mice with B2M knockout exhibit aberrant axonal and dendritic outgrowth, abnormal synapse density and expanded ipsilateral projection [36, 49–51]. In our current study, hPSCs with B2M knockout are regularly differentiated into neurons with no observed aberrant synaptic density and neurite outgrowth. Whole-cell patch clamping further reveals that B2M knockout hPSC-derived neurons attain the normal capacity to fire trains-of-action potentials and display spontaneous postsynaptic currents *in vitro*. It is therefore reasonable to conclude that hypoimmunogenic hPSCs hold normal intrinsic programs to differentiate into morphologically and electrophysiologically mature neurons and these neurons could organize into functional neural circuits. In the *in vivo* context, lack of surface expression of major histocompatibility complex molecules expression in cell types other than neurons, such as astrocytes or microglia, might lead to a malfunction of the immune milieu, which subsequently causes aberrant neuronal development, maturation and neuronal transmission. Indeed, major histocompatibility complex molecules expression in microglia is required in synaptic development [52]. On the other hand, B2M deficient mice fail to express major histocompatibility complex class I products, resulting in systemic iron overload and consequently hepatocytes necrosis and abnormal metabolic function [53]. Here, the hypoimmunogenic hPSC-derived hepatocytes are phenotypically normal and possess natural metabolic functions. This again supports the hypothesis that the expression patterns of major histocompatibility complex molecules in hepatocytes might be not essential for their normal function. Of note, ectopic expression of membrane-bound or soluble HLA-G proteins could ameliorate abnormal overactivation of NK cells and antigen presenting cells, which could serve as a pledge of supporting normal development and function of derivatives of these hypoimmunogenic hPSCs after allograft transplantations [17]. In the future, *in vivo* transplantation studies in animal models or clinical trials will be expected in order to propagate our current study to apply these universal cell sources for cell therapeutics.

Conclusions

In the current study, we present evidences and show that hypoimmunogenic hPSCs with variable expression patterns of HLA molecules and immune compromising spectrums retain their normal self-renewal capacity and could be efficiently differentiated into functional and mature lineage cells, such as electrophysiologically active neurons, beating cardiomyocytes and albumin secreting hepatocytes. These

hypoimmunogenic hPSCs hold great promise to serve as unlimited universal cell sources for cell therapeutics.

Materials And Methods

Cell culture and differentiation

Undifferentiated human H9 ES cells (WA09, WiCell) and hypoimmunogenic hPSCs were maintained on irradiated mouse embryonic fibroblasts (MEF) in hESCM containing DMEM/F12, 20% knockout serum replacer, 1 ´ non-essential amino acids, 1 ´ GlutaMAX, and 0.1 mM b-mercaptoethanol at 37°C with 5% CO_2 as previously described [17,54]. Fibroblast growth factor 2 (FGF2, 4 ng/mL, Peprotech) was added when refreshing medium. Cells were manually passaged at 1:6 split ratio every 5 days with dispase digestion. For neural differentiation, we used previously described protocols [38-40]. In brief, cells were cultured in hESCM : neural induction medium (NIM) (1:1) for 3 days supplemented with 2 μM SB431542 (Stemgent) and 200 nM LDN193189 (Stemgent), followed by 4 days with 2 μM SB431542 and 200 nM LDN193189 in NIM, then 5 days in NIM. Cells were pipetted up and maintained in suspension culture on day 12, then 8 days in NIM. On day 20, cells were plated on laminin-coated coverslip for neurons in neural differentiation medium (NDM) with 10 ng/ml BDNF (Peprotech), 10 ng/ml GDNF (Peprotech) and 10 ng/ml IGF (Peprotech). NIM contains DMEM/F12: neuralbasal medium (1:1), N2 supplement and B27 (complete with Insulin). NDM contains neuralbasal medium, N2 supplement and B27 (complete with Insulin), 200 mM ascorbic acid, and 1 mM cAMP. For cardiomyocyte differentiation, procedures were described previously [44-45]. In brief, cells were cultured in hESCM on the day -4 to -1. Then cells were cultured in RPMI/B27 medium (Insulin minus, Gibco) supplemented with 12 μM CHIR99021 (Selleck) for 1 day, followed by 2 days in RPMI/B27 medium (Insulin minus), then 2 days supplemented with 5 μM IWP2 (Selleck) in RPMI/B27 medium (Insulin minus), then 2 days in RPMI/B27 medium (Insulin minus), then refreshing every 3 days with RPMI/B27 (complete with Insulin). For hepatic differentiation, we made minor modifications based on previously described protocols [47-48]. Briefly, cells were cultured in hESCM on the day -3 to 0. Then cells were cultured in RPMI/B27 medium (Insulin minus, Gibco) supplemented with 100 ng/ml Activin A (Peprotech) for 3 days, followed by 4 days with 20 ng/ml BMP2 (Peprotech) and 30 ng/ml FGF-4 (Peprotech) in RPMI/B27 (complete with Insulin, Gibco) medium, then 6 days with 20 ng/ml HGF (Peprotech) and KGF (Peprotech) in RPMI/B27 (complete with Insulin), then 8 days with 20 ng/ml Oncostatin-M (R&D Systems) in hepatocyte culture media (Lonza) supplemented with SingleQuots (without EGF).

Electrophysiology

Hypoimmunogenic hPSC- and hESC-derived neurons were recorded at 8-10 weeks with whole-cell patch clamp at room temperature using a MultiClamp 700B amplifier (Molecular Devices, Sunnyvale, CA, USA). Recording micropipettes (tip resistance 3-6 MΩ) were filled with internal solution composed of (in mM): 140 K-gluconate, 1 EGTA, 2 $MgCl_2$, 4 MgATP, 0.3 NaGTP, 10 HEPES and 0.1 $CaCl_2$ (pH 7.4). The bath was perfused with artificial cerebrospinal fluid (ACSF) composed of (in mM): 119 NaCl, 1.8 KCl, 2.4 $CaCl_2$, 10

glucose, 1 NaH_2PO_4, 26.2 $NaHCO_3$ and 1.2 $MgCl_2$ (pH 7.4). For voltage-clamp recordings, cells were clamped at -70 mV. Spontaneous postsynaptic currents were recorded for at least 3 min. For current-clamp recordings, voltage responses were evoked from -10 to +80 pA in 10 pA intervals. Single action potential (AP) properties were calculated from the first evoked AP in response to a depolarizing step. Quantitative analysis was done using Clampfit software (Molecular Devices, SanJose, CA) and Mini Analysis Software (Synaptosoft). For cellular action potentials of cardiomyocytes, it was recorded at day 30-35. Recording micropipettes (tip resistance 3-6 MΩ) were filled with internal solution composed of (in mM): 10 EGTA, 1 $MgCl_2$, 3 MgATP, 10 HEPES and 120 KCl (pH 7.2). The bath was perfused with Tyrode's solution composed of (in mM): 135 NaCl, 5.4 KCl, 1.8 $CaCl_2$, 10 glucose and 0.3 Na_2HPO_4, 0.3 KH_2PO_4 and 10 HEPES (pH 7.35). Quantitative analysis was done using Clampfit software. The following was the criteria used for classifying observed APs into ventricular, atrial and nodal-like cells [55]. Cells with ventricular-like action potentials typically displayed a more negative maximum diastolic potential, a rapid action potential upstroke, and a distinct plateau phase. Atrial-like cells were distinguished from ventricular-like cells by the absence of a distinct plateau during repolarization but typically exhibited spontaneous activity that was higher in frequency than that observed in ventricular cells. Nodal-like cells were distinguished by maximum diastolic potentials that were less negative than those of ventricular- and atrial-like cells, smaller amplitude action potentials, characterized as a slower action potential upstroke, and a pronounced phase 4 depolarization preceding the action potential upstroke.

Immunofluorescence

Cells on coverslips were fixed in 4% paraformaldehyde for 20-30 min at room temperature. After three washes in PBS, cells were blocked in blocking buffer (PBS, 10% donkey serum, 0.1% Triton X-100) for 1 h at room temperature. Cells were incubated with primary antibodies at 4℃ overnight, washed three times with PBS and incubated with a secondary antibody for 1 h at room temperature. Then cells were washed and stained with Hoechst 33258 (Sigma D9542) for 5-10 mins. Primary antibodies used in this study were: OCT4 (Santa Cruz), SOX2 (R&D System), PAX6 (Covance), TUJ1 (Sigma), Synapsin1 (Sigma), NKX2.5 (Santa Cruz), cTnT (Abcam), α-actinin (Sigma-Aldrich), MLC2a (Synapic systems), AFP (GeneTex), ALB (GeneTex).

Flow cytometry

Cells were dissociated into single cell with accutase at 37℃ for 3 min and then followed by the FACS Kit (BD bioscience) treatment according to the manufacturer's instructions. Samples were sorted on a FACSVerse flow cytometer (BD Biosciences) and analyzed in CytExpert. Antibodies used in this study were: PAX6 (DSHB), ALB (GeneTex), and isotype control mouse IgG (eBioscience).

Teratoma formation

hESCs and hypoimmunogenic hPSCs were injected subcutaneously on the back of NOD/SCID immunodeficient mice (Shanghai MODEL ORGANISMS, China). After 2 months, mice with teratomas were sacrificed. Then teratomas were stained with H&E. All animal experiments were conducted in accordance

with the Guide for the Care and Use of Animals for Research Purposes and approved by the Tongji University Animal Care Committee.

Periodic acid Schiff staining.

Periodic acid Schiff (PAS) staining was performed by using the PAS staining kit (abcam) according to the manufacturer's instructions.

Indocyanine green uptake and release

Indocyanine green (ICG) (Sigma) was dissolved in DMSO at 5 mg/ml. Cells were exposed to ICG diluted freshly in culture medium to 1 mg/ml for 30 min at 37℃. After washing with PBS, cells were refilled with the culture medium and incubated for 6 h. Then the uptake and release of cellular ICG was examined.

ALB secretion

The protein level of ALB in culture medium was determined with an ELISA Kit (Elabscience) according to the manufacturer's instructions.

Statistical analyses

Data were presented as mean ± SEM. The statistical significance of differences was determined by unpaired two-tailed Student's *t*-test. $P<0.05$ was considered statistically significant.

Abbreviations

hPSCs
hypoimmunogenic human pluripotent stem cells
HLA
human leukocyte antigen
CTLA4
cytotoxic T lymphocyte antigen 4
PD-L1
programmed death ligand-1
MHC
major histocompatibility complex
NOD/SCID
non-obese diabetic/severe combined immune-deficient
H&E
hematoxylin-eosin
AP
action potential
RMP

resting membrane potential
cTnT
cardiac troponin T
APD
action potential duration
APA
action potential amplitude
ICG
Indocyanine green
PAS
periodic acid Schiff.

Declarations

Acknowledgements

This work was supported by grants from the National Key Research and Development Program of China (Grant no. 2018YFA0108000, 2019YFA0110300, 2021YFA1100400 and 2021YFC2701400), the National Natural Science Foundation of China (Grant No. 8205020, 32000689, and 31872760), the Science and Technology Commission of Shanghai Municipality (19JC1415100 and 21140902300), the Major Program of Development Fund for Shanghai Zhangjiang National Innovation Demonstration Zone (Stem Cell Strategic Biobank and Clinical Translation Platform of Stem Cell Technology, ZJ2018-ZD-004).

Author Contributions

X.Z. and L.L. conceived and designed the project. Y.C. and Y.Z. performed the experiments. Z.Z. performed the bioinformatics analyses. J.X., Y.F. and L.M. helped with cardiac differentiation. Y.C., X.Z. and L.L. wrote the manuscript. All authors discussed the results and commented on the manuscript.

Ethics approval and consent to participate

All animal experiments were conducted in accordance with the Guide for the Care and Use of Animals for Research Purposes and approved by the Tongji University Animal Care Committee.

Consent for publication

Not applicable.

Competing Interests

The authors declare no competing interests.

Availability of data and materials

All data generated or analyzed during this study are included in this published article.

References

1. Yamanaka S. Pluripotent Stem Cell-Based Cell Therapy-Promise and Challenges[J]. Cell Stem Cell. 2020;27(4):523–31.
2. Thomson JA, Itskovitz-Eldor J, Shapiro SS, et al. Embryonic stem cell lines derived from human blastocysts. Science. 1998;282(5391):1145–7.
3. Takahashi K, Tanabe K, Ohnuki M, et al. Induction of pluripotent stem cells from adult human fibroblasts by defined factors. Cell. 2007;131(5):861–72.
4. Lipsitz YY, Timmins NE, Zandstra PW. Quality cell therapy manufacturing by design. Nat Biotechnol. 2016;34:393–400.
5. Blair NF, Barker RA. Making it personal: the prospects for autologous pluripotent stem cell-derived therapies. Regen Med. 2016;11:423–5.
6. Chakradhar S. An eye to the future: researchers debate best path for stem cell-derived therapies. Nat Med. 2016;22:116–9.
7. Smith DM. Assessing commercial opportunities for autologous and allogeneic cell-based products. Regen Med. 2012;7:721–32.
8. Lipsitz YY, Bedford P, Davies AH, et al. Achieving efficient manufacturing and quality assurance through synthetic cell therapy design. Cell Stem Cell. 2017;20:13–7.
9. van Berlo JH, Molkentin JD. An emerging consensus on cardiac regeneration. Nat Med. 2014;20:1386–93.
10. Larosa DF, Rahman AH, Turka LA. The innate immune system in allograft rejection and tolerance. [J]. J Immunol. 2007;178(12):7503.
11. Braud VM, Allan D, O'Callaghan CA, et al. HLA-E binds to natural killer cell receptors CD94/NKG2A, B and C[J]. Nature. 1998;391(6669):795–9.
12. Lee N, Llano M, Carretero M, et al. HLA-E is a major ligand for the natural killer inhibitory receptor CD94/NKG2A[J]. Proceedings of the National Academy of Sciences, 1998, 95(9):5199-5204.
13. Ferreira L, Meissner TB, Tilburgs T, et al. HLA-G: At the Interface of Maternal–Fetal Tolerance[J]. Trends Immunol. 2017;38(4):272–86.
14. Pazmany L, Mandelboim O, Valesgomez M, et al. Protection from Natural Killer Cell-Mediated Lysis by HLA-G Expression on Target Cells[J]. Science. 1996;274(5288):792–5.
15. Gornalusse GG, Hirata RK, Funk SE, et al. HLA-E-expressing pluripotent stem cells escape allogeneic responses and lysis by NK cells. Nat Biotechnol. 2017;35(8):765–72.
16. Han X, Wang M, Duan S, et al. Generation of hypoimmunogenic human pluripotent stem cells. Proc Natl Acad Sci USA. 2019;116(21):10441–6.

17. Shi L, Li W, Liu Y, et al. Generation of hypoimmunogenic human pluripotent stem cells via expression of membrane-bound and secreted β2m-HLA-G fusion proteins. Stem Cells. 2020 Nov;38(11):1423–37.
18. Jaiswal S, Jamieson CH, Pang WW, et al. CD47 is upregulated on circulating hematopoietic stem cells and leukemia cells to avoid phagocytosis. Cell. 2009 Jul 23;138(2):271-85.
19. Deuse T, Hu X, Gravina A, et al. Hypoimmunogenic derivatives of induced pluripotent stem cells evade immune rejection in fully immunocompetent allogeneic recipients. Nat Biotechnol. 2019;37(3):252–8.
20. Braciale TJ. Antigen processing for presentation by MHC class I molecules. Curr Opin Immunol. 1992;4(1):59–62.
21. Feng Q, Shabrani N, Thon JN, et al. Scalable generation of universal platelets from human induced pluripotent stem cells. Stem Cell Reports. 2014;3(5):817–31.
22. Lu P, Chen J, He L, et al. Generating hypoimmunogenic human embryonic stem cells by the disruption of beta 2-microglobulin. Stem Cell Rev Rep. 2013;9(6):806–13.
23. Riolobos L, Hirata RK, Turtle CJ, et al. HLA engineering of human pluripotent stem cells. Mol Ther. 2013;21(6):1232–41.
24. Wang D, Quan Y, Yan Q, Morales JE, Wetsel RA. Targeted disruption of the beta2-microglobulin gene minimizes the immunogenicity of human embryonic stem cells. STEM CELLS TRANSLATIONAL MEDICINE. 2015;4(10):1234–45.
25. Arce-Gomez B, Jones EA, Barnstable CJ, Solomon E, Bodmer WF. The genetic control of HLA-A and B antigens in somatic cell hybrids: requirement for beta2 microglobulin. Tissue Antigens. 1978;11(2):96–112.
26. Xu H, Wang B, Ono M, et al. Targeted disruption of HLA genes via CRISPR-Cas9 generates iPSCs with enhanced immune compatibility. Cell Stem Cell. 2019;24(4):566–78.
27. Rong Z, Wang M, Hu Z, et al. An effective approach to prevent immune rejection of human ESC-derived allografts. Cell Stem Cell. 2014;14(1):121–30.
28. Drukker M, Katz G, Urbach A, et al. Characterization of the expression of MHC proteins in human embryonic stem cells. Proc Natl Acad Sci U S A. 2002 Jul 23;99(15):9864-9.
29. Johansson JS. Effect of inflammatory cytokines on major histocompatibility complex expression and differentiation of human neural stem/progenitor cells[J]. STEM CELLS; 2008.
30. Pick M, Ronen D, Yanuka O, et al. Reprogramming of the MHC-I and Its Regulation by NFκB in Human-Induced Pluripotent Stem Cells[J]. Stem Cells, 2012, 30(12).
31. Sabha M Jr, Emirandetti A, Cullheim S, et al. MHC I expression and synaptic plasticity in different mice strains after axotomy. Synapse. 2008;62:137–48.
32. Oliveira AL, Thams S, Lidman O, et al. A role for MHC class I molecules in synaptic plasticity and regeneration of neurons after axotomy. Proc Natl Acad SciUSA. 2004;101:17843–8.

33. Corriveau RA, Huh GS, Shatz CJ. Regulation of class I MHC gene expression in the developing and mature CNS by neural activity. Neuron. 1998;21:505–20.
34. Huh GS, Boulanger LM, Du H, et al. Functional requirement for class I MHC in CNS development and plasticity. Science. 2000;290:2155–9.
35. Goddard CA, Butts DA, Shatz CJ. Regulation of CNS synapses by neuronal MHC class I. Proc Natl Acad SciUSA. 2007;104:6828–33.
36. Elmer BM, Mcallister AK. Major histocompatibility complex class I proteins in brain development and plasticity.[J]. Trends Neurosci. 2012;35(11):660–70.
37. Rothenberg BE, et al. beta2 knockout mice develop parenchymal iron overload: A putative role for class I genes of the major histocompatibility complex in iron metabolism.[J]. Proceedings of the National Academy of Sciences of the United States of America; 1996.
38. Chi L, Fan B, Feng D, et al. The dorsoventral patterning of human forebrain follows an activation/transformation model. Cereb Cortex. 2016a;27:2941–54.
39. Chi L, Fan B, Zhang K, et al. Targeted differentiation of regional ventral neuroprogenitors and related neuronal subtypes from human pluripotent stem cells. Stem Cell Reports. 2016b;7:941–54.
40. Zhu X, Bo L, Ai Z, et al. A Robust Single Primate Neuroepithelial Cell Clonal Expansion System for Neural Tube Development and Disease Studies[J]. Stem Cell Reports. 2015;6(2):228–42.
41. Fisher SA, Brunskill SJ, Doree C, et al. Stem cell therapy for chronic ischaemic heart disease and congestive heart failure.[J]. Cochrane Database of Systematic Reviews. 2014;12(4):CD007888.
42. Nn A, Eg B.. Stem cell therapy in heart failure: Where do we stand today?[J]. Biochimica et Biophysica Acta (BBA) - Molecular Basis of Disease, 1866(4).
43. Nguyen PK, Rhee JW, Wu JC.. Adult Stem Cell Therapy and Heart Failure, 2000 to 2016: A Systematic Review[J]. Jama Cardiol, 2016, 1(7):831–41.
44. Laflamme MA, Chen KY, Naumova AV, et al. Cardiomyocytes derived from human embryonic stem cells in pro-survival factors enhance function of infarcted rat hearts[J]. Nature Biotechnology.
45. Lian X, Zhang J, Azarin SM, et al. Directed cardiomyocyte differentiation from human pluripotent stem cells by modulating Wnt/betacatenin signaling under fully defined conditions. Nat Protoc. 2013;8(1):162–75.
46. Burridge PW, Matsa E, Shukla P, et al. Chemically defined generation of human cardiomyocytes. Nat Methods. 2014 Aug;11(8):855–60.
47. Chen Y-F. Chien-Yu Tseng, Hsei-Wei Wang, et al. Rapid generation of mature hepatocyte-like cells from human induced pluripotent stem cells by an efficient three-step protocol. [J]. Hepatology, 2012, 55(4).
48. Song Z, Cai J, Liu Y, et al. Efficient generation of hepatocyte-like cells from human induced pluripotent stem cells[J]. Cell Research (2009):1233–1242.
49. Glynn MW, Elmer BM, Garay PA, et al Needleman LA, El-Sabeawy F, McAllister AK. MHCI negatively regulates synapse density during the establishment of cortical connections. Nat Neurosci.

2011;14:442–51.
50. Bilousova T, Dang H, Xu W, et al. Major histocompatibility complex class I molecules modulate embryonic neuritogenesis and neuronal polarization[J]. J Neuroimmunol. 2012;247(1-2):1–8.
51. Boulanger L, Shatz C. Immune signalling in neural development, synaptic plasticity and disease. Nat Rev Neurosci. 2004;5:521–31.
52. Schafer D, Lehrman E, Kautzman A, et al. Microglia Sculpt Postnatal Neural Circuits in an Activity and Complement-Dependent Manner[J]. Neuron. 2012;74:691–705.
53. Muckenthaler MU, Rodrigues P, Macedo MG, et al. Molecular analysis of iron overload in beta2-microglobulin-deficient mice.[J]. Blood Cells Molecules and Diseases. 2004;33(2):125–31.
54. Zhang X, Huang CT, Chen J, et al. Pax6 is a human neuroectoderm cell fate determinant. Cell Stem Cell. 2010;7(1):90–100.
55. Zhang J, Wilson GF, Soerens AG, et al. Functional Cardiomyocytes Derived From Human Induced Pluripotent Stem Cells[J]. Circul Res. 2009;104(4):e30.

Figures

Figure1

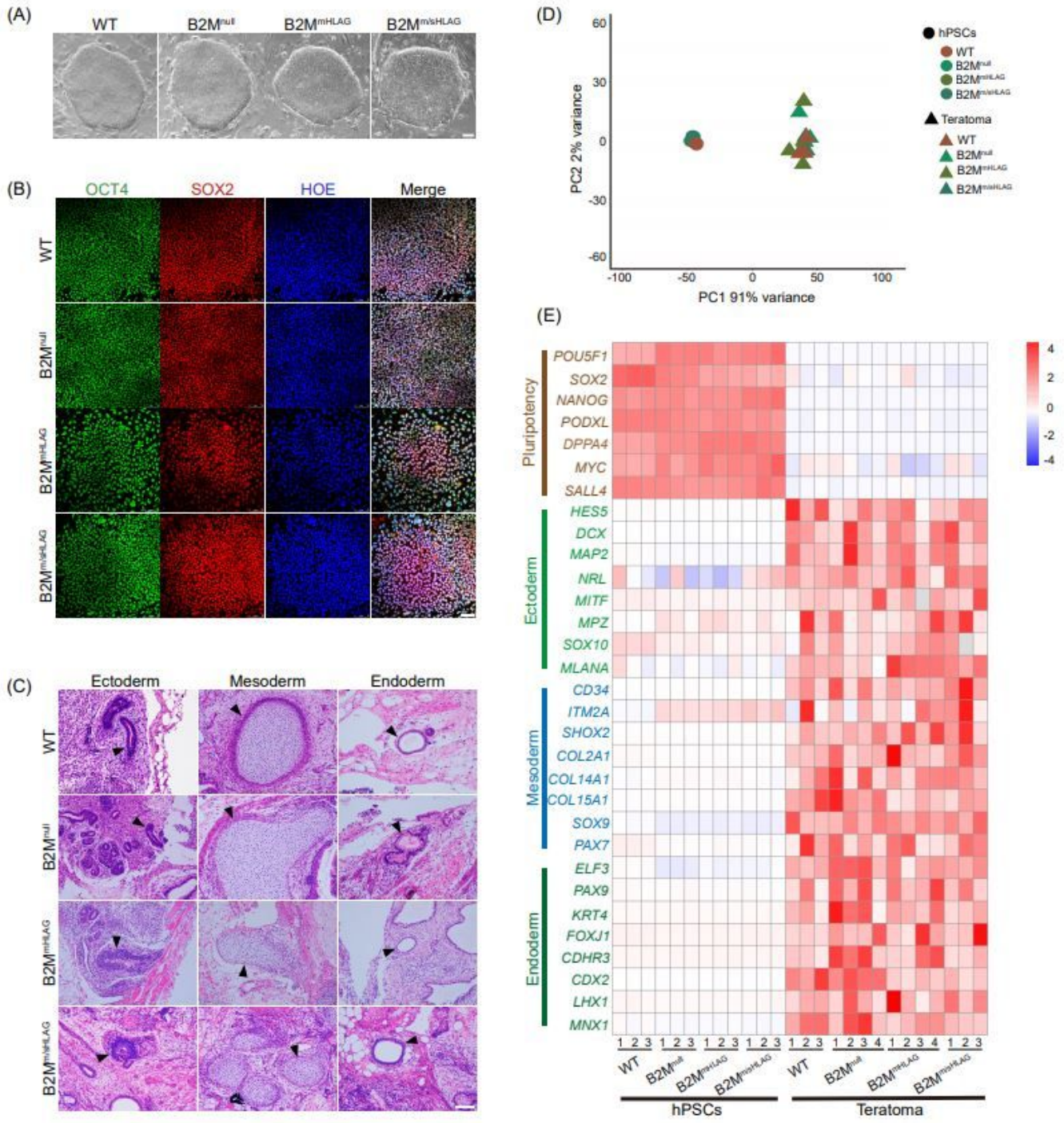

Figure 1

Hypoimmunogenic human pluripotent stem cells (hPSCs) retain normal self-renewal and multi-lineage differentiation

(**A**) Brightfield images of wild type (WT) and hypoimmunogenic hPSCs cultured more than 30 passages. Scale bar, 100 μm. WT, undifferentiated human H9 ES cells; B2M^{null}, biallelic lesion of B2M gene to

remove all surface expression of classical and nonclassical HLA class I molecules; $B2M^{mHLAG}$, biallelic homologous recombination of nonclassical HLA-G1 to the B2M loci to knockout B2M while express membrane-bound β2m-HLA-G1 fusion proteins; $B2M^{m/sHLAG}$, ectopic expression of soluble and secreted β2m-HLA-G5 fusion proteins in $B2M^{mHLAG}$ hPSCs.

(**B**) Immunostaining of OCT4 and SOX2 in WT and hypoimmunogenic hPSCs. Nuclei were stained with Hoechst (HOE). Scale bar, 75 μm.

(**C**) H&E staining identified three germ layers in teratomas from WT and hypoimmunogenic hPSCs. Typical tissues were marked by arrowheads (left panel, neural tube-like tissues for ectoderm; middle panel, cartilage like tissues for mesoderm; right panel, intestine like tissues for endoderm). Scale bar, 100 μm.

(**D**) Principal component analysis (PCA) plot of WT, hypoimmunogenic hPSCs and teratomas formed by WT and hypoimmunogenic hPSCs. PCA showed two different clusters, hypoimmunogenic hPSCs clustered with WT hPSCs but not their teratomas.

(**E**) A heatmap of differentially expressed signature genes from RNA-seq data of pluripotency, ectoderm, mesoderm and endoderm in WT, hypoimmunogenic hPSCs and their teratomas.

Figure2

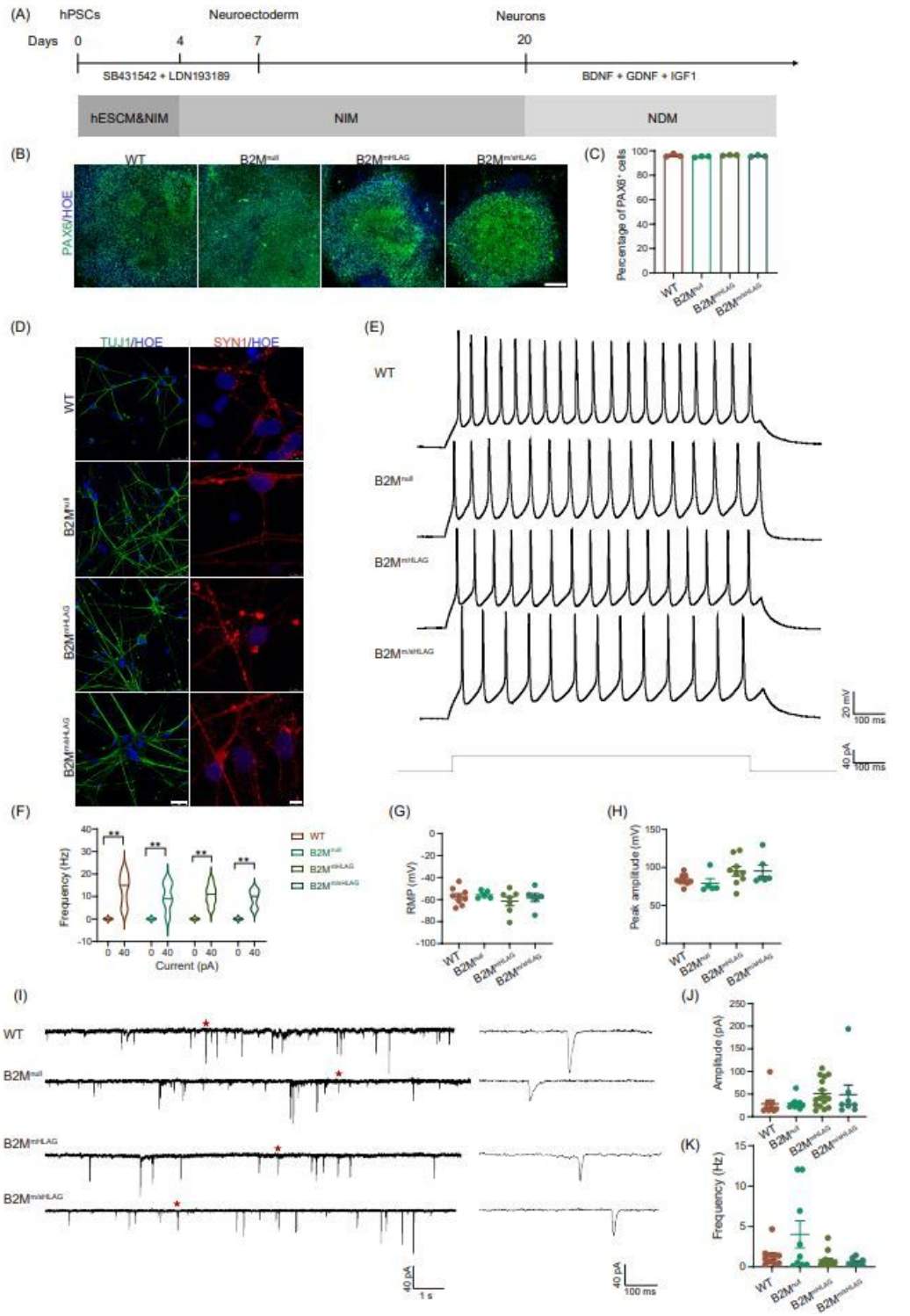

Figure 2

Differentiation of hypoimmunogenic hPSCs into electrophysiologically mature neuronal networks

(**A**) Schematic of the protocol and stages for the neural differentiation of hPSCs.

(**B**) Representative neural tube-like rosette structures formed by $PAX6^+$ neuroepithelial cells. Scale bar, 100 μm.

(**C**) Flow cytometry analysis showing the percentage of $PAX6^+$ cells on day 12 neural differentiation of WT and hypoimmunogenic hPSCs. Data are presented as mean ± SEM. $p > 0.05$, n=3, Student's *t* test.

(**D**) Representative immunofluorescence images of TUJ1 and SYN1 in WT and hypoimmunogenic hPSCs-derived neurons. Scale bars, left, 25 μm; right, 5 μm.

(**E**) Representative traces from neurons derived from hypoimmunogenic and WT hPSCs firing repetitive APs during depolarizing constant-current injections. Current step is shown in the bottom panel.

(**F**) Violin plots of frequency-current (F-I) among firing neurons (current injection=0 & 40pA). Data are presented as mean ± SEM. ** $p < 0.01$, n (WT) =8, n ($B2M^{null}$) =5, n ($B2M^{mHLAG}$) =11, n ($B2M^{m/sHLAG}$) =6, Student's *t* test.

(**G** and **H**) Resting membrane potentials (G) and peak amplitudes (H) of neurons derived from hypoimmunogenic and WT hPSCs. Parameters were calculated from the first evoked spike. Data are presented as mean ± SEM. For resting membrane potentials, n (WT) =9, n ($B2M^{null}$) =5, n ($B2M^{mHLAG}$) =7, n ($B2M^{m/sHLAG}$) =6. For peak amplitudes, n (WT) =9, n ($B2M^{null}$) =5, n ($B2M^{mHLAG}$) =9, n ($B2M^{m/sHLAG}$) =6. Both $p > 0.05$, Student's *t* test.

(**I**) Left, representative voltage-clamp recording from neurons derived from hypoimmunogenic and WT hPSCs with spontaneous synaptic input (Vm = -70 mV). Right, zoom-in of the region in left marked by the red five-pointed star, containing one postsynaptic event.

(**J** and **K**) Amplitudes (J) and frequencies (K) of spontaneous postsynaptic currents of neurons derived from hypoimmunogenic and WT hPSCs. Data are represented as mean ± SEM. $p > 0.05$, n (WT) =10, n ($B2M^{null}$) =9, n ($B2M^{mHLAG}$) =16, n ($B2M^{m/sHLAG}$) =8, Student's *t* test.

Figure3

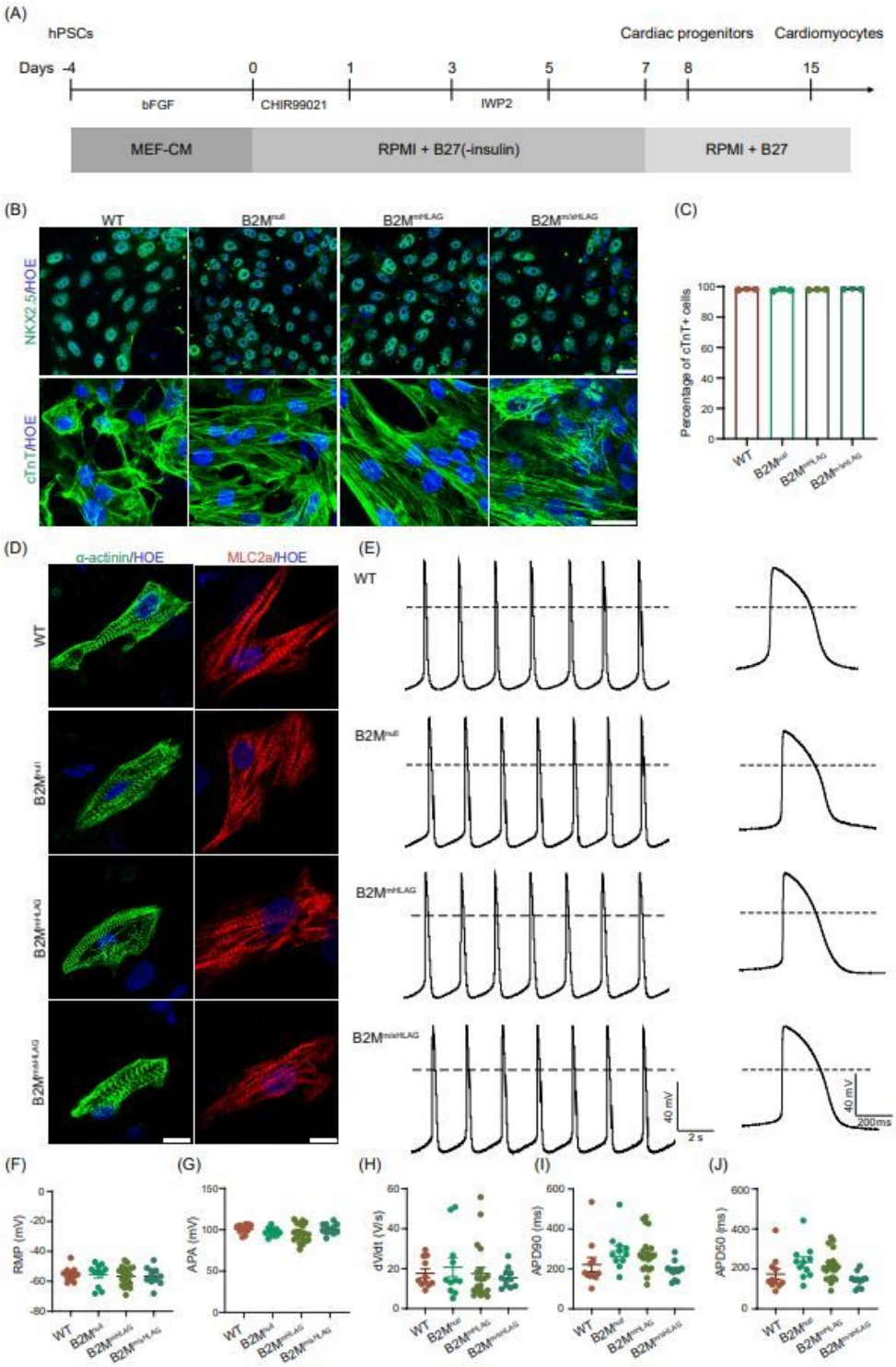

Figure 3

Characterization of cardiomyocytes generated from hypoimmunogenic hPSCs

(**A**) Schematic of the protocol and stages for the cardiac differentiation of hPSCs.

(**B**) Representative immunofluorescence images of NKX2.5 on day 8 and cTnT at 3 weeks of cardiac differentiation of WT and hypoimmunogenic hPSCs. Scale bars, 25 μm.

(**C**) Quantification of differentiated $cTnT^{+}$ cardiomyocyte-like cells. Data are represented as mean ± SEM. $p > 0.05$, n=3, Student's *t* test.

(**D**) Representative immunofluorescence images of sarcomere organization by α-actinin and MLC2a staining. Scale bars, 25 μm.

(**E**) Representative recordings of ventricular-like action potentials using whole-cell patch clamp from cardiomyocytes differentiated from WT and hypoimmunogenic hPSCs. Dotted line indicates 0 mV. Right, single action potential at an expanded timescale taken from traces on the left.

(**F-J**) Comparison of rest membrane potential (RMP, F), action potential amplitude (APA, G), maximal rate of depolarization (dV/dt_{max}, H), action potential duration at 90% repolarization (APD, I) and 50% repolarization (J) in cardiomyocytes differentiated from WT and hypoimmunogenic hPSCs. Data are represented as mean ± SEM. $p > 0.05$, n (WT) =11, n ($B2M^{null}$) =11, n ($B2M^{mHLAG}$) =20, n ($B2M^{m/sHLAG}$) =11, Student's *t* test.

Figure4

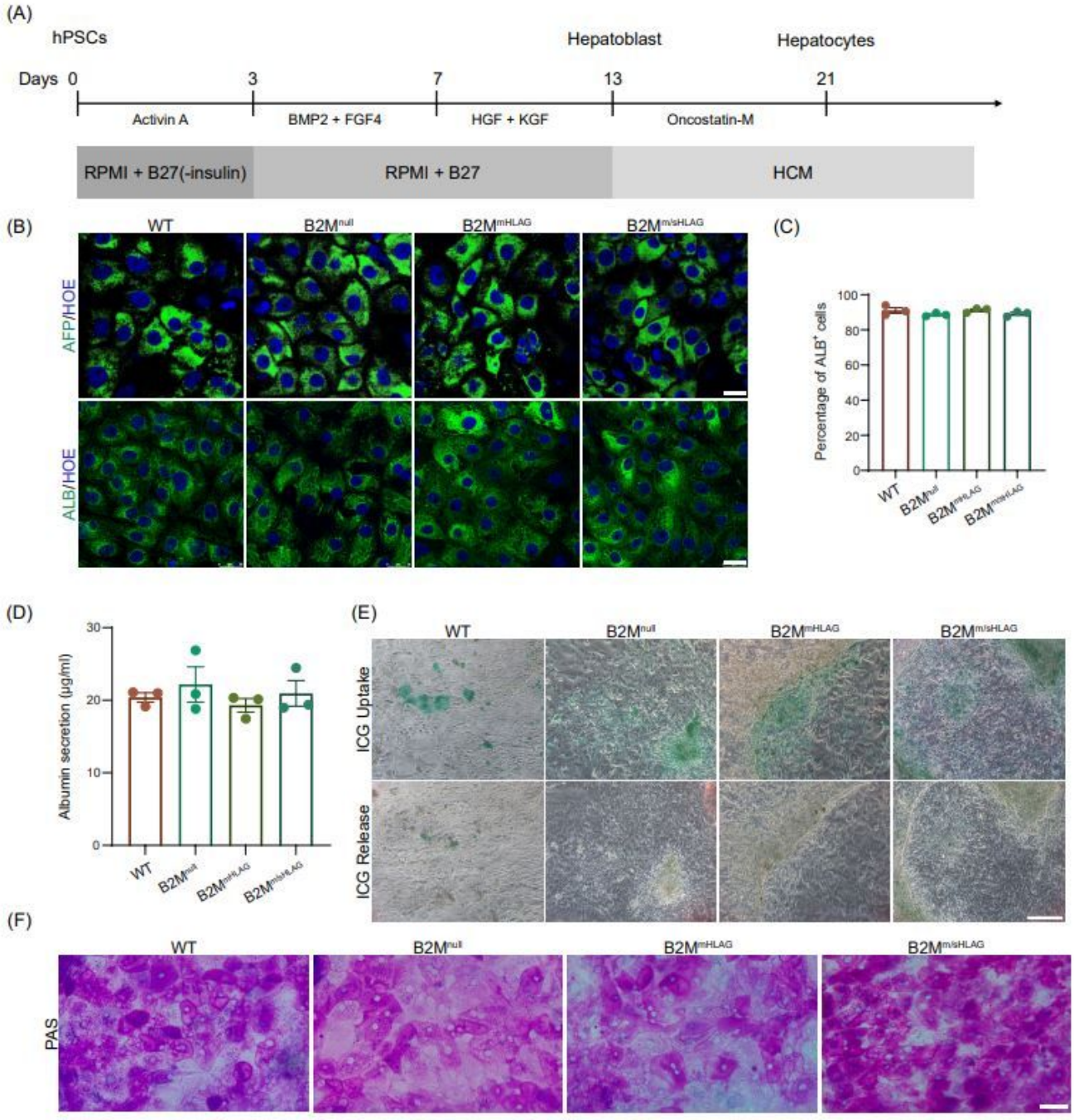

Figure 4

Functional analysis of the hepatocytes derived from WT and hypoimmunogenic hPSCs

(**A**) Schematic of the protocol and stages for the hepatic differentiation of hPSCs.

(**B**) Representative immunofluorescence images of alpha fetoprotein (AFP), and albumin (ALB) in hepatocytes differentiated from WT and hypoimmunogenic hPSCs. Scale bars, 25 μm.

(**C**) Quantification analyses of the percentages of ALB^+ cells on day 21 hepatic differentiation of WT and hypoimmunogenic hPSCs. Data are represented as mean ± SEM. $p > 0.05$, n=3, Student's *t* test.

(**D**) Quantification of ALB secretion from WT- and hypoimmunogenic hPSCs-derived hepatocytes. Data are represented as mean ± SEM. $p > 0.05$, n=3, Student's *t* test.

(**E**) ICG uptake and release assay of WT- and hypoimmunogenic hPSCs-derived hepatocytes. Scale bar, 250 μm.

(**F**) Glycogen synthesis analysis by PAS staining on day 21 hepatic differentiation of WT and hypoimmunogenic hPSCs. Scale bar, 50 μm.

Supplementary Files

This is a list of supplementary files associated with this preprint. Click to download.

- WTVideo1.avi
- B2MnullVideo2.avi
- B2MmHLAGVideo3.avi
- B2MmsHLAGVideo4.avi